Journal Pre-proof

Constructing Ag_2O nanoparticle modified TiO_2 nanotube arrays for enhanced photocatalytic performances

Junwei Hou, Jingyi Zhou, Yafeng Liu, Ye Yang, Shixin Zheng, Qingyao Wang

PII: S0925-8388(20)32857-7

DOI: https://doi.org/10.1016/j.jallcom.2020.156493

Reference: JALCOM 156493

To appear in: *Journal of Alloys and Compounds*

Received Date: 17 June 2020

Revised Date: 10 July 2020

Accepted Date: 21 July 2020

Please cite this article as: J. Hou, J. Zhou, Y. Liu, Y. Yang, S. Zheng, Q. Wang, Constructing Ag_2O nanoparticle modified TiO_2 nanotube arrays for enhanced photocatalytic performances, *Journal of Alloys and Compounds* (2020), doi: https://doi.org/10.1016/j.jallcom.2020.156493.

Junwei Hou and **Qingyao Wang**: contributed the central idea, analyzed most of the data, and wrote the initial draft of the paper. **Jingyi Zhou** and **Yafeng Liu:** carried out the synthesis, characterizations of hybrid samples. The remaining authors contributed to refining the ideas, carrying out additional analyses and finalizing this paper. All authors discussed the results and provided input to the manuscript.

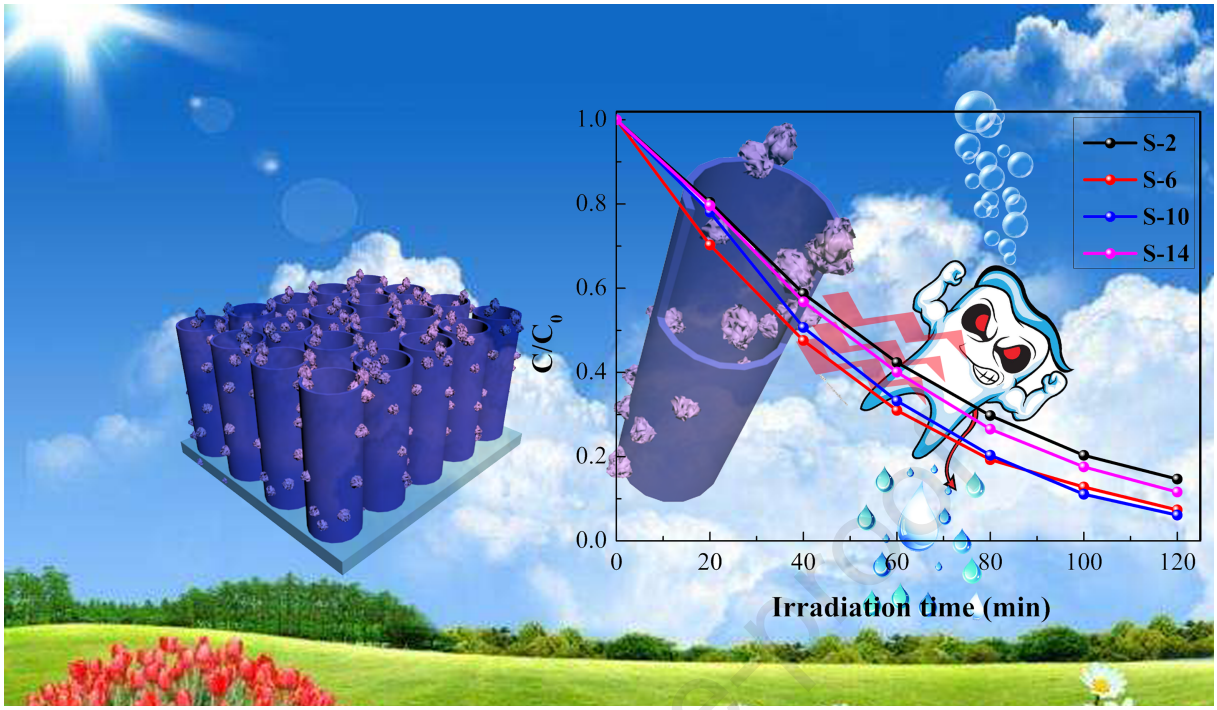

Constructing Ag_2O nanoparticle modified TiO_2 nanotube arrays for enhanced photocatalytic performances

Junwei Hou [a,*], Jingyi Zhou [a], Yafeng Liu [a], Ye Yang [a], Shixin Zheng [b], Qingyao Wang[b,*]

[a] State Key Laboratory of Heavy Oil Processing, China University of Petroleum (Beijing), Beijing, 102249, China

[b] School of Chemistry and Materials Science, Ludong University, Yantai, 264025, China

Email: Junweihou@cupk.edu.cn (J. Hou) and wangqingyao0532@163.com (Q.Wang)

Abstract

Currently, the silver-based semiconductor modified TiO_2 nanotube arrays (TiO_2 NTA) for the improved photocatalytic treatment of industrial waste water have been a hot topic. The simple synthesis and environmental application of photocatalysts with excellent photocatalytic ability is still a big challenge. Herein, We reported the successive ionic layer adsorption and reaction (SILAR) preparation of Ag_2O nanoparticles on TiO_2 NTA surfaces. The different deposition cycles were performed to investigate the influence of Ag_2O deposition amounts on the photoelectrochemical activity. Results revealed that the S-10 fabricated with 10 SILAR cycles had the impressive photocatalytic and photoelectric conversion performances. The visible light photovoltage and photocurrent of S-10 electrode were -0.20 V and 463.2 $\mu A/cm^2$. Moreover, the photocatalytic degradation efficiencies of MO, RhB and MB dyes achieved 67.40%, 59.19% and 93.89%, respectively. Further increasing the irradiation time, the mineralization degree of organic dyes were improved up to 71.28%, 60.31%, and 92.58% after 6 h solar irradiation. Cr(VI) ions were also dramatically removed by photocatalysts. The remarkable photocatalytic performance of Ag_2O/TiO_2 NTA would

exhibit attractive prospect in the industrial waste water purification.

Key words: Ag_2O nanoparticles; TiO_2 NTA; SILAR; Photocatalytic performance.

1. Introduction

Dyeing and printing industry is a traditional and crucial commercial model in every country, which discharges massive waste water including methylene blue (MB), rhodamine B (RhB), and methyl orange (MO) into river, lake and sea [1~4]. The organic azo dye could produce carcinogenic aromatic compounds. Therefore, the direct discharge of organic dye waste water is inhibited, and the degradation even mineralization of dye molecules could significantly reduce the toxicity. Compared with the common physical, chemical and biological methods, the photocatalytic progress is an ideal green strategy by the solar energy utilization to achieve the decomposition of dyes into CO_2 and H_2O molecules [5~8]. Photocatalyst is the most important factor for the complete degradation of toxic dyes, and TiO_2 nanoparticles are recognized to be the prospective photocatalysts because of the low cost, high stability and excellent photocatalytic ability since the discovery of hydrogen generation on TiO_2 powders by water splitting [9, 10]. Recently, the two dimensional (2D) TiO_2 NTA film composed by 1D nanotubes attracted intense attention, and the TiO_2 NTA photocatalyst showed higher photocatalytic capacity than other morphologies [11]. Our group also investigated the preparation and photocatalytic pollutant degradation of TiO_2 NTA grown on Ti foils [12], Ti meshes [13] and Ti foams [14], and the suitable synthesis condition guaranteed the uniform microstructure and outstanding photocatalytic property. However, the poor visible

light response is the biggest restriction of solar energy utilization and photocatalytic property of TiO_2 NTA. Therefore, many methods such as noble metal/semiconductor modification and ion doping were applied to further extend the solar absorption region and reduce the charge carrier recombination [15, 16]. Semiconductors such as CdS [17], Bi_2WO_4 [18], CuO [19], et al. were deposited on TiO_2 NTA surface to enhance the solar utilization efficiency, revealing the outstanding photocatalytic performance in the dye degradation. However, the sensitizers containing heavy metal ions may cause the secondary pollution during the photocatalytic progress. Some green Ag-based semiconductors such as Ag_3PO_4 [20], AgX (X= Cl, Br, I) [21], Ag_2MoO_4 [22] and so on are suitable sensitizers due to the avirulence, high solar absorption coefficient and photocatalytic capacity. Ag_2O nanoparticles with the narrow band gap of 1.2 eV cause the intense focus, and the previous research testified the excellent photocatalytic activity and compatibility with TiO_2. For examples, Ren [23] prepared Ag_2O/TiO_2 composites for the MO photocatalytic degradation, and the degradation rate constant was improved up 20 times of pure TiO_2. Prof. Liu [24] revealed the promoting effect of Ag_2O on TiO_2 nanobelts in the solar absorption and photocatalytic decomposition of MO under UV/visible light irradiation. Liu [25] and Deng [26] reported the Ag_2O nanoparticle sensitization of TiO_2 NTA by electrochemical and microwave-assisted reduction deposition, and the photocatalyst showed excellent photocatalytic performances in various dyes. The previous investigation results inferred that Ag_2O nanoparitlces could significantly induce the photocatalytic capacity enhancement of TiO_2 NTA, but the systematic researches about the mechanism and

active species are still needed to be further illuminated. In this paper, Ag_2O nanoparticles were synthesized on TiO_2 NTA surfaces by the SILAR strategy. The solar response, photoelectric activity and photocatalytic remediation of dyes and Cr (VI) in waste water by the composite photocatalyst were investigated in detail. We also tentatively explored the active specie and carrier transportation mechanism by the free radical scavenger and ESR experiments. The photocatalytic study of Ag_2O/TiO_2 NTA would provide the theory and technology guide for the printing and dyeing waste water purification.

2. Experimental section

2.1. Materials and reagents

Ti foils with superhigh purity (> 99.8%) were purchased from Sinopharm Chemical Reagent CO., Ltd. Ammonium fluoride (NH_4F), sodium hydroxide (NaOH) and silver nitrate ($AgNO_3$) were purchased from China National Pharmaceutical Group Co., Ltd. Deionized water was home-made in high purity water production facility. All reagents were analytically pure without further purification.

2.2. Fabrication of Ag_2O nanoparticle-sensitized TiO_2 NTA photocatalysts

The TiO_2 NTA was firstly grown on Ti foils by the anodization method according to our previous investigation [27, 28]. Briefly, Ti foils were cleaned in isopropanol, methanol and acetone for 10 min, respectively, and then activated in $HF/HNO_4/H_2O$ (volume ration= 1:4:5) solution for 2 min. Ti foils were anodized in organic ethylene glycol electrolyte including 3.0 vol.% H_2O and 0.5 wt.% NH_4F at 60 V for 2 h. After the anodization, the prepared TiO_2 NTA was calcinated at 450 ^oC to enhance the

crystallization.

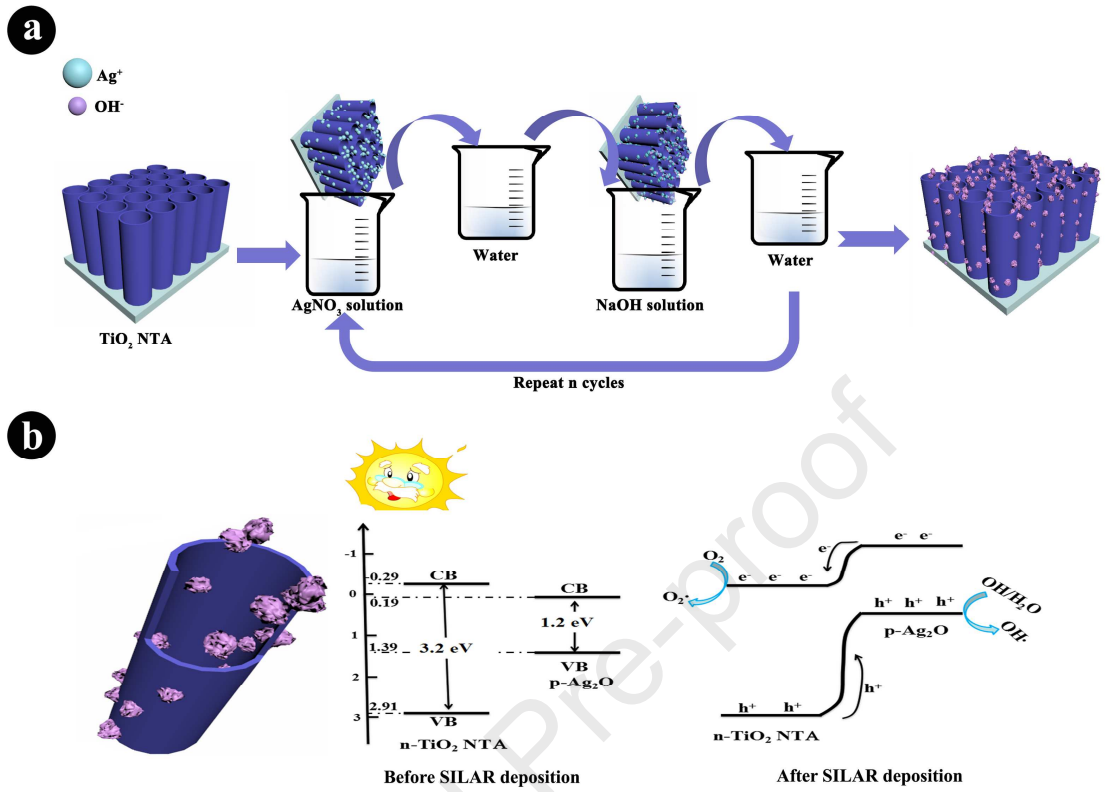

Scheme 1 The preparation (a) and photocatalytic mechanism (b) of Ag_2O/TiO_2 NTA.

Ag_2O nanoparticles were deposited on TiO_2 NTA by the SILAR method, and the preparation progress was exhibited in Scheme 1a. In the typical preparation progress, TiO_2 NTA were placed in 0.1 mol/L $AgNO_3$ solution for 5 min to achieve the abundant Ag^+ adsorption, and then cleaned by deionized water. Afterwards, the sample was transferred into 0.1 mol/L NaOH solution for another 5 min, and then cleaned by deionized water again. The above dipping progress was named as one Ag_2O deposition cycle, and the Ag_2O/TiO_2 NTA photocatalysts synthesized with 2, 6, 10 and 14 cycles were labeled as S-2, S-6, S-10 and S-14, respectively. Finally, all as-prepared samples were annealed at 160 ^oC in a vacuum oven.

2.3. Characterization

The phase composition and chemical valance of samples were analyzed by X-ray diffraction (XRD, Bruker D8) and X-ray photoelectron microscopy (XPS, ESCALAB Xi^+). Scanning electron microscope (SEM, SU8010) and transmission electron microscope (TEM, Talos F200X G2) was used to obtain the morphology. HAADF-STEM and EDX elemental mapping analysis were carried out at 200 kV. The solar absorption activity was evaluated by UV-Vis diffuse reflectance spectra (DRS, UV-2550) and incident photon to current efficiency (IPCE, CEL-QPCE1000).

2.4. Photoelectric conversion test

The photoelectric characterization was operated in a quartz photocell with the standard three electrode system in 0.2 mol/L Na_2SO_4 electrolyte, whereas the samples served as the work electrode, Pt wires and Ag/AgCl electrodes worked as the counter and reference electrodes, respectively. The sample was irradiated from the lateral wall by visible light from a 500 W Xe lamp (CEL-S500) with a UV-cutoff filter ($\lambda \geq$ 420 nm). With the assistance of electrochemical workstation (CHI 660E), the transient photocurrent, electrochemical impedance spectroscopy (EIS) and photovoltage were recorded.

2.5. Photocatalytic performance test

The photocatalytic capacity of samples was studied by the purification of MB, RhB, MO dyes and Cr (VI) in 0.1 mol/L Na_2SO_4 and NaCl solution under solar irradiation, respectively. The photocatalytic test was performed in a two electrode system. A 500 W Xe lamp (CEL-S500) with AM 1.5 filter was used as the light source, samples were placed 10 cm distance with Xe lamp and the light intensity was characterized to

be about 80 kW/m^2. Before the photocatalytic test, 30 min magnetic stirring was carried out for the adsorption-desorption balance. For the organic dyes decomposition, the absorbance of MO, RhB and MB was recorded by 721 UV-vis spectrophotometer at the characteristic absorbance peak of 552, 464 and 664 nm, respectively. For the Cr (VI) removal, the diphenylcarbazide spectrum method was used to investigate the ion concentration and photocatalytic efficiency.

For the deep investigation about active species in the photocatalytic dye degradation, the free radical scavenge experiments and electron spin resonance spectrometer (ESR, MiniScope MS5000) were used to confirm reactive species. Moreover, the total organic carbon (TOC, 4200) was applied to study the mineralization degree of dyes.

3. Results and discussion

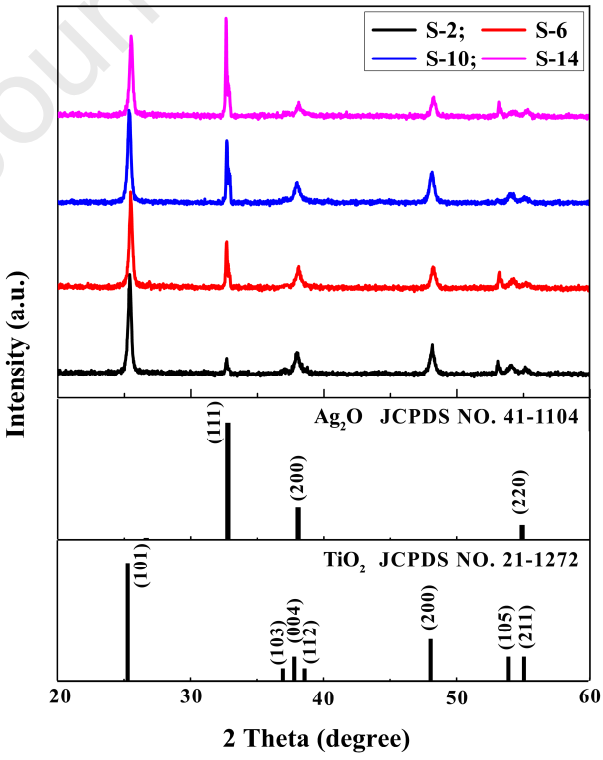

Fig. 1 XRD patterns of the samples.

The phase composition of the TiO_2 NTA after Ag_2O deposition was displayed in Fig. 1. According to the standard diffraction patterns of anatase TiO_2 and Ag_2O, the typical TiO_2 diffraction peaks could be clearly observed, and the peaks at 32.79°, 38.07° and 54.90° can be assigned to the (1 1 1), (2 0 0) and (2 2 0) lattice planes of cubic Ag_2O (JCPDS NO. 41-1104). It could be seen that the diffraction peak intensity is gradually increased with the increment of SILAR deposition cycles, and this phenomenon could be totally attributed to the increasing deposition amount of Ag_2O.

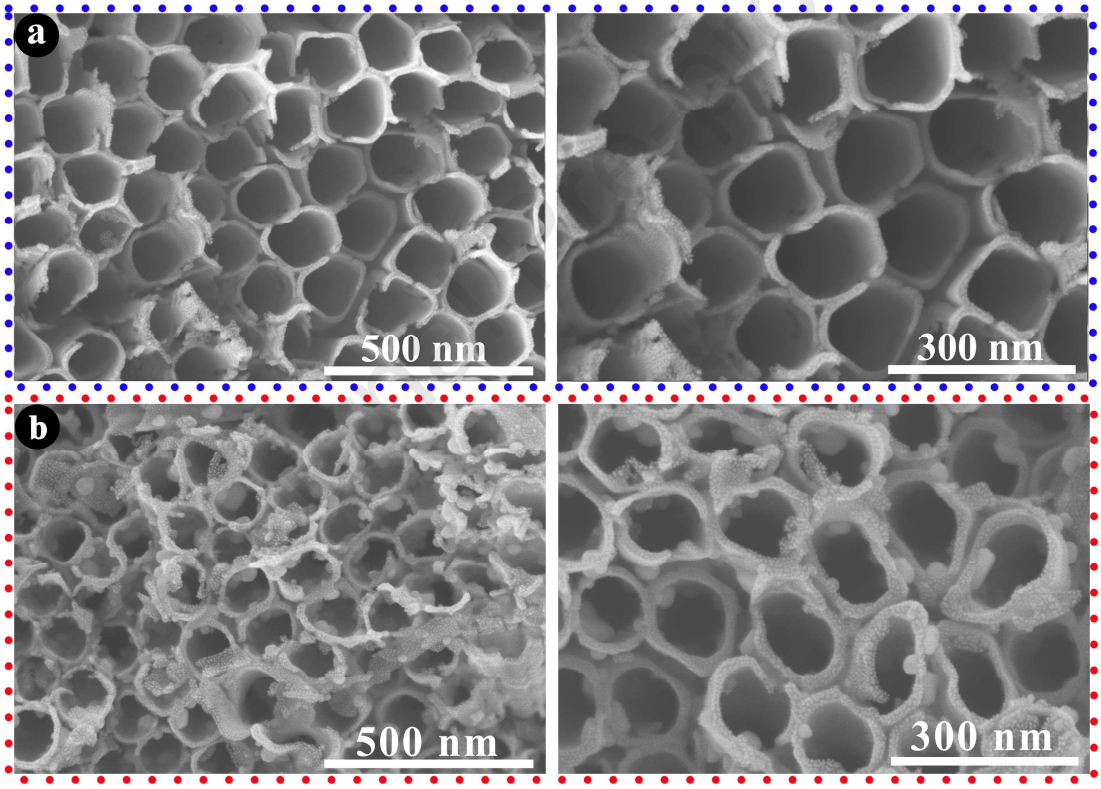

Fig. 2 SEM images of TiO_2 NTA (a) and S-10 (b).

The SEM images of TiO_2 NTA before/after Ag_2O deposition were investigated in Fig. 2. As displayed in Fig. 2a, the pure TiO_2 NTA exhibits uniform tubular microstructure with a smooth surface. Careful observation shows that the wall thickness and diameter of TiO_2 NTA are calculated to be around 18 nm and 140 nm,

which are similar with our previous report [9]. The diameter and wall thickness were mainly governed by the electrolyte and anodization voltage. Previous researches revealed that the ethylene glycol organic electrolyte is beneficial to the clean and ordered TiO_2 NTA with high photocatalytic and photoelectrochemical activity. The Ag_2O deposition could be obviously noticed in Fig. 2b, and small Ag_2O nanoparticles with average size of 25 nm cover the TiO_2 NTA top surface. Interestingly, Ag_2O nanoparticles are also deposited on inner nanotube walls, illuminating the successful preparation of Ag_2O by SILAR deposition strategy.

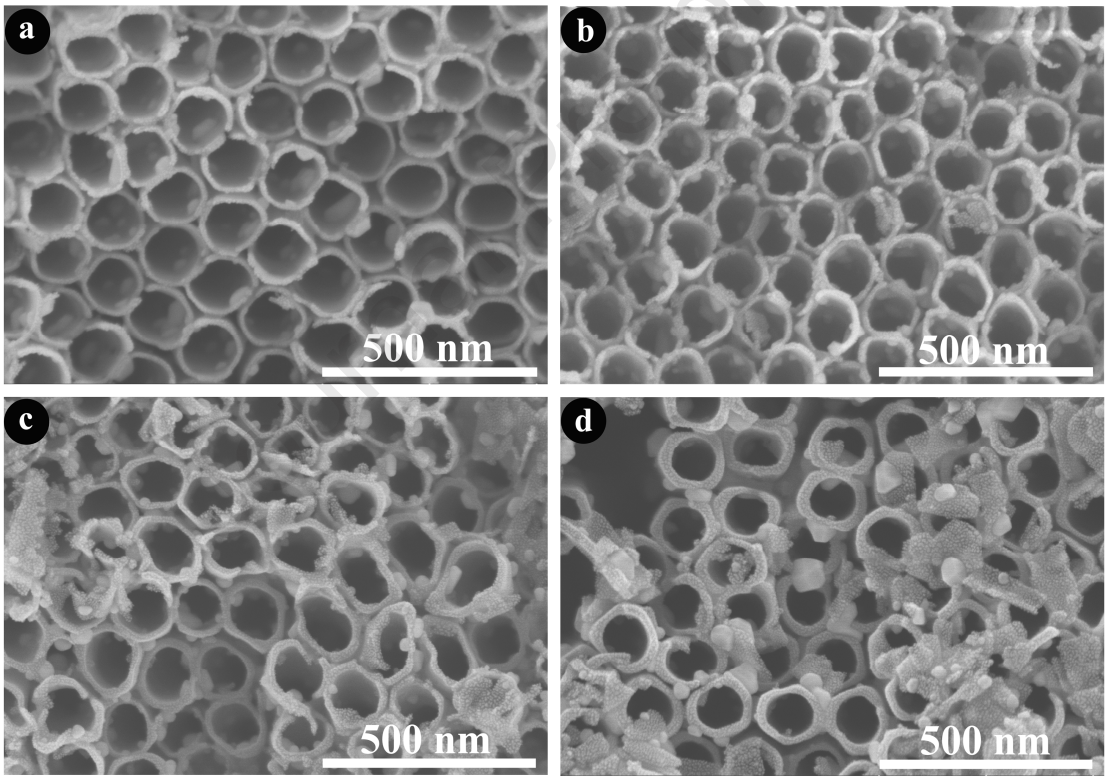

Fig. 3 SEM images of S-2 (a), S-6 (b) S-10 (c) and S-14 (d).

The influence of SILAR deposition cycles on the morphology were tested by SEM in Fig. 3. The obvious deposition amount change could be observed, and the massive Ag_2O nanoparticles were deposited on TiO_2 NTA surface along the SILAR deposition increment. As shown in Fig. 3a, few Ag_2O nanoparticles were observed at the top

surface of TiO_2 NTA, but the careful observation could find the Ag_2O nanoparticles adsorbing at the inner surface of nanotubes. Increasing the deposition SILAR, the deposited Ag_2O was steadily on the increase, and especially more and bigger Ag_2O nanoparticles were synthesized with the 14 SILAR cycle deposition.

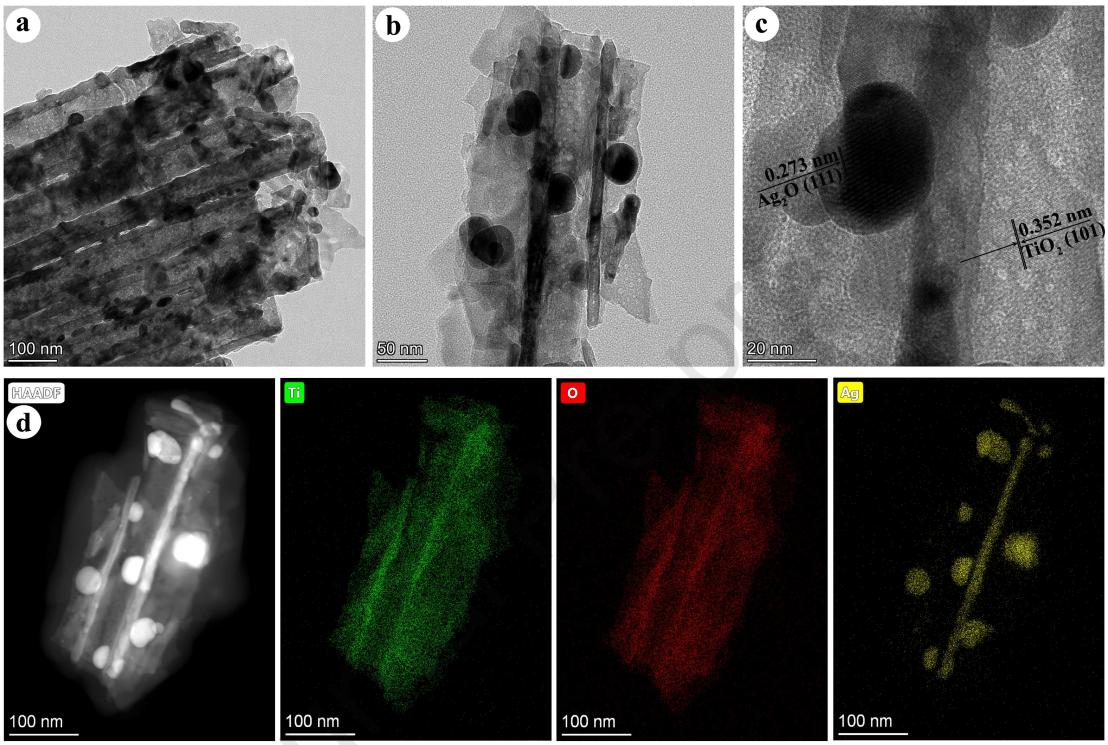

Fig. 4 TEM (a, b), HRTEM images (c) and elemental mappings (d) of S-10.

The microstructure of Ag_2O/TiO_2 NTA was investigated by TEM and HRTEM images. The clear tubular structure could observed in Fig. 4a and 4b, and the Ag_2O nanoparticles at the tube surface were also noticed. The HRTEM image in Fig. 4c was further tested to confirm the formation of Ag_2O, and the clear lattice fringes can be observed. The interplanar spacings of 0.352 nm and 0.273 nm of crystal lattices are fairly close to the (1 0 1) plane of TiO_2 and (1 1 1) plane of Ag_2O, respectively, which further illuminating the Ag_2O nanoparticles at TiO_2 NTA. Moreover, the corresponding elemental mappings of Ag_2O/TiO_2 NTA in Fig. 4d suggest the homogeneous distribution of Ag_2O nanoparticles.

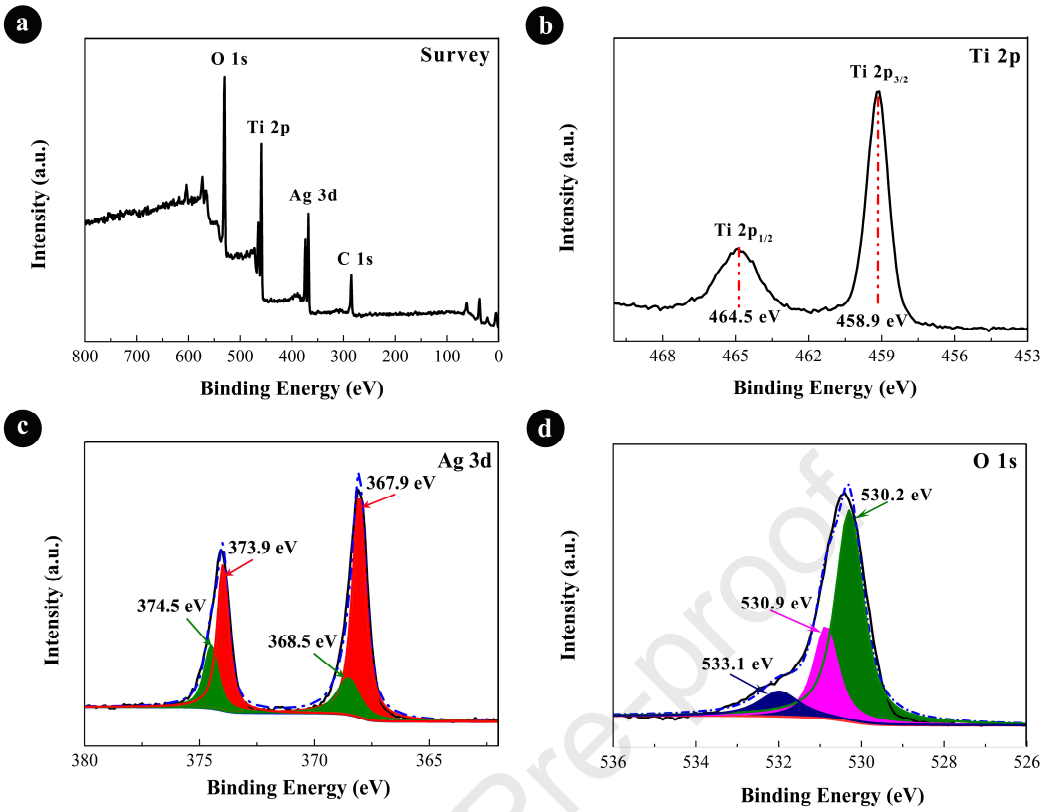

Fig. 5 XPS spectra of survey (a), Ti 2p (b), Ag 3d (c) and O 1s (d).

The chemical composition and element valence state were studied by the XPS technique in Fig. 5. As shown in Fig. 5a , Ti, O, Ag and C elements are presented at the S-10 surface in the survey spectrum. The C element is derived from the residual organic electrolyte or adsorbed CO_2 and other containing carbon compounds, and the C 1s at 284.5 eV serves as the reference to calibration. The Ti $2p_{1/2}$ and Ti $2p_{3/2}$ bands of S-10 are located at 464.5 eV and 458.9 eV as shown in Fig. 5b, which are same with the report of TiO_2 NTA [9]. The asymmetric double peaks of Ag at 373.6 eV and 367.4 eV could be split into four peaks. After the peak resolving, the peaks at 368.5 eV and 374.5 eV are ascribed to metallic Ag^0, and the peaks at 367.9 eV and 373.9 eV are ascribed to Ag $3d_{3/2}$ and Ag $3d_{5/2}$ of Ag^+ in Ag_2O, which are in good agreement with Ag_2O [26]. Furthermore, the large O 1s XPS peak could be split into three ones,

and the peaks at 533.1 eV, 530.9 eV and 530.2 eV are attributed to the adsorbed oxygen and crystal oxygen of Ag-O and Ti-O, respectively [26]. The XPS results confirm the successful deposition of Ag_2O on TiO_2 NTA, illuminating the effective contact of two semiconductors.

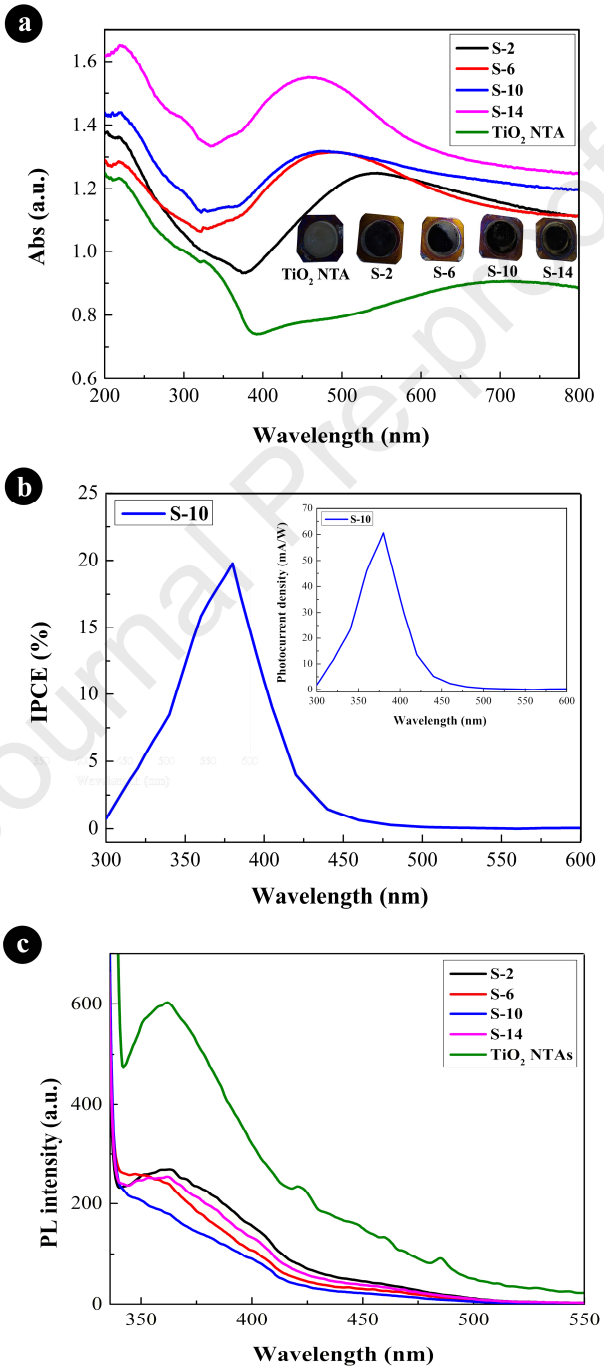

Fig. 6 DRS spectra (a), IPCE (b) and PL (c) of the as-prepared samples.

The solar response, IPCE and PL spectra of all samples were studied by DRS in Fig. 6. Pure TiO_2 NTA could only harvest UV light with high solar energy because of the limited large band gap. After the Ag_2O SILAR deposition, the absorbance in the visible light region could be significantly enhanced, and the absorption intensity is gradually enhanced along the increment of SILAR deposition cycles. Moreover, the solar absorption ability of the as-prepared samples was further confirmed by the IPCE in Fig. 6b. We could notice that the photoelectric conversion of S-10 sample was performed under the irradiation of visible light with the wavelength less than 500 nm. The maximum IPCE value (19.77%) is obtained at 380 nm, and the value at 500 nm still achieves 0.13%. The excellent visible light response activity guarantees the application of Ag_2O/TiO_2 NTA with high solar utilization and photoelectrochemical performances in photocatalysts and solar cells. Moreover, the electron recombination performances of samples were presented in Fig. 6c, and the clear result indicated the high recombination chance of electron/hole pairs in TiO_2 NTA , revealing the low electron utilization efficiency. The significant enhancement is observed after the Ag_2O sensitization, and the SILAR cycle dramatically influences the electron recombination performance. The SILAR deposition increment reduces the rapid recombination at the initial stage, but the recombination becomes strong after 10 deposition cycles. The severe recombination in S-14 is mainly ascribed to the massive Ag_2O deposition on the TiO_2 NTA surface that induces the efficient charge carrier transportation.

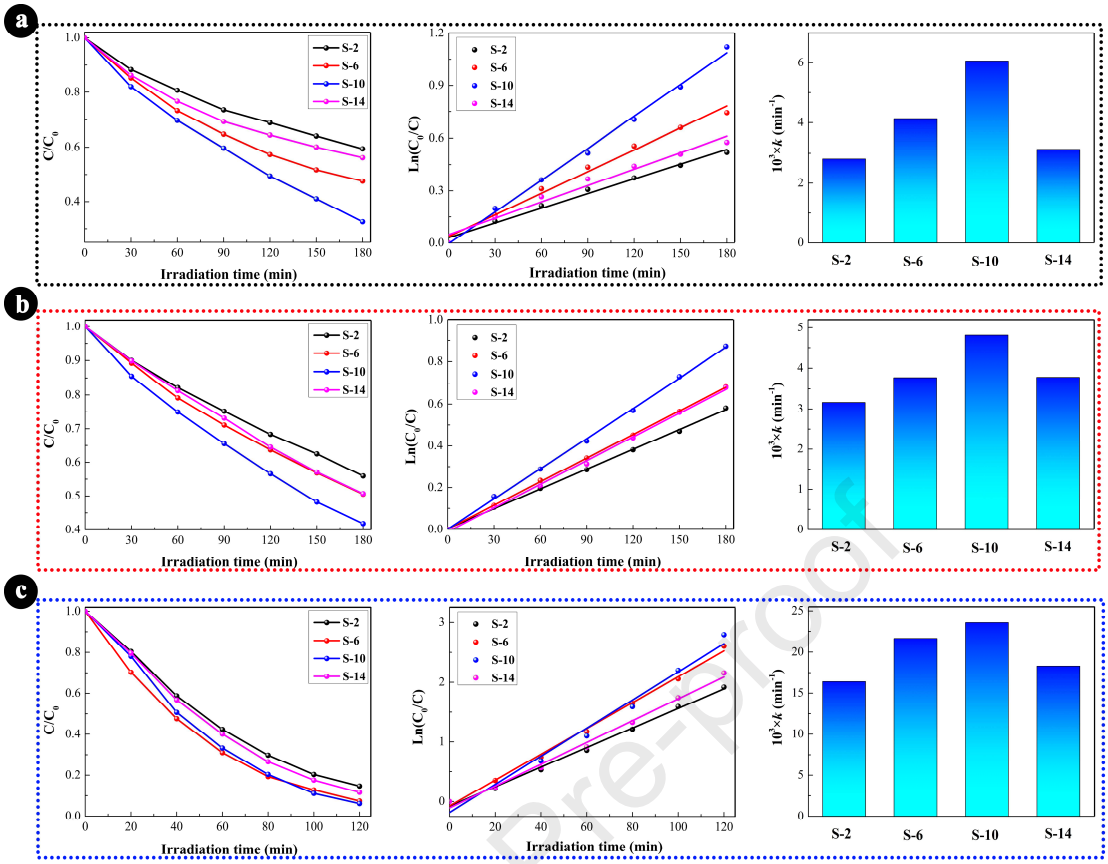

Fig. 7 PEC degradation of MO (a), RhB (b) and MB (c) by the as-prepared photocatalysts.

The photocatalytic performances of the as-prepared photocatalysts for the dye decoloration were investigated. In the photocatalytic tests, MO, RhB and MB dyes were selected to simulate the dyeing and textile waste water, and the photocatalytic data was analyzed in Fig. 7. MO dye molecules could be decolorized after 3 h solar irradiation, and the S-10 sample shows the most excellent photocatalytic activity. The photocatalytic efficiency (67.40%) is even 1.66, 1.29 and 1.54 folds of S-2, S-6 and S-14, respectively. The photocatalytic kinetics progress is provided by the first-order fitting equation, and the photocatalytic efficiency $Ln(C_0/C)$ *vs* irradiation time shows linear correlation with correlation coefficient (R^2 >0.98). The photocatalytic rate constant has the similar trend with final photocatalytic efficiency, and the S-10

photocatalyst has the biggest value (6.06×10^{-3} min^{-1}). Similarly with the decoloration of MO dyes, RhB and MB dyes were also decomposed by the solar photocalalysis in Fig. 7b and 7c. The S-10 sample shows the optimal photocatalytic performance both in RhB and MB dyes, and the photocatalytic kinetic progresses of RhB and MB decomposition are also displayed. The photocatalytic efficiencies and rate constants for RhB and MB dyes are 59.19%/180 min, 93.89%/120 min and 4.81×10^{-3} min^{-1}, 2.36×10^{-2} min^{-1}. The influence of SILAR cycles on photocatalytic performance could be summarized as following: The photocatalytic ability is improved with SILAR cycle increment before 10 cycles, and then dramatically reduces with the further increment. The 10 SILAR cycle deposition is the suitable experimental parameter for Ag_2O deposition, and the sensitizer deposition amount greatly decides the solar harvesting and electron transportation. The suitable deposition amount is beneficial to achieve the balance in solar harvesting and electron transportation, and the detailed discussion and explanation were reported in our previous research [29].

The photocatalytic performance comparison with other groups was listed in Table 1. The previous investigation reveals the excellent photocatalytic ability of Ag_2O/TiO_2 photocatalysts, and the hybrid photocatalyst could achieve the effective photocatalytic decomposition of various organic pollutants under UV or visible light irradiation. Although the photocatalytic efficiency of Ag_2O/TiO_2 NTs in our work is seemed weaker than some reported data, the photocatalyst addition amount in the experiment is about 1 mg, which is only 1% of traditional photocatalyst addition. The Prof. Tang's review [30] indicated that the photocatalytic performance in different investigation

groups couldn't be directly compared due to the different light source, light power intensity, irradiation time, dye kind and concentration, photocatalyst addition amount and so on.

Table 1 Ag_2O/TiO_2 nanoparticles for photocatalytic decoloration of organic pollutants

Photocatalysts	Preparation methods	Light sources	Pollutants	Efficiency	Refs.
Ag_2O/TiO_2 NTA	SILAR deposition	Solar light	MO RhB MB	67.40% 59.19% 93.89%	This work
Ag_2O/TiO_2 NTA	Electrodeposition	Solar light	Acid orange 7	100%	[25]
Ag_2O/TiO_2 NTA	Anodization	UV–vis light	Phenol	77%	[31]
Ag_2O/TiO_2 microspheres	Hydrothermal synthesis	UV light	MO	93%	[32]
Ag_2O/TiO_2 nanobelts	Chemical precipitation	Visible light	MO	80%	[33]
Ag_2O/TiO_2 NTA	Microwave reduction	Solar light	MB	98.9%	[34]
Ag_2O/TiO_2 heterostructure	Precipitation	Visible light	MB	98.3%	[35]
Ag_2O/TiO_2	Solvothermal synthesis	Visible light	MB	88.2%	[36]
Ag_2O/TiO_2	Chemical precipitation	UV light	MO	98.2%	[23]
Ag_2O/TiO_2	Precipitation	UV light	RhB	99%	[37]

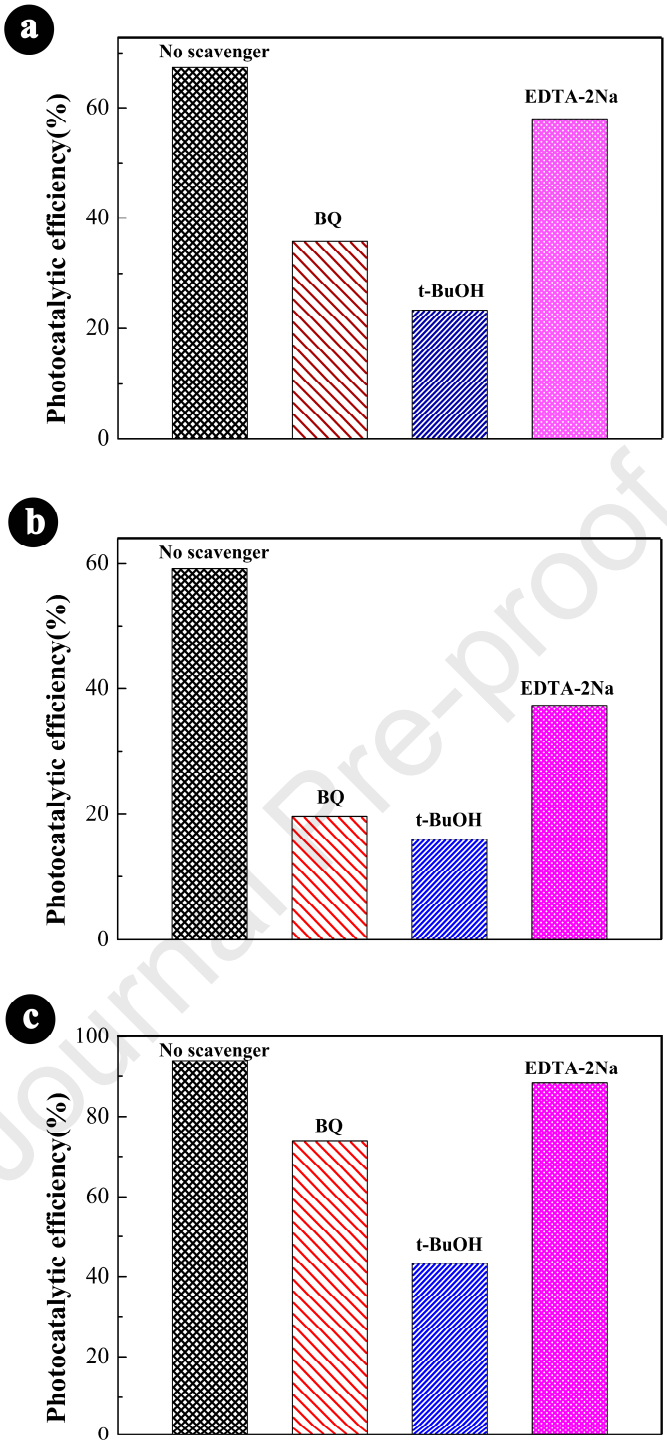

Fig. 8 The photocatalytic performance after adding scavengers in MO (a), RhB (b) and MB (c) solutions.

The active species of the photocatalytic decoloration were explored by adding free radical scavengers, and the final efficiency was shown in Fig. 8. It could be obviously

observed that the t-BuOH addition significantly inhibits the photocatalytic decomposition of dyes, and the photocatalytic performances of three dyes become poor. The decoloration ratios of MO, RhB and MB are 34.54%, 27.10% and 46.18% of results without scavenger addition, indicating the •OH radical is the main active specie for dye decomposition. Except for t-BuOH, the addition of BQ and EDTA-2Na also reduces the dye photocatalytic decoloration, and $•O_2^-$ radical also plays vital roles in photocatalytic reaction. It is well known that $•O_2^-$ radicals could transform into •OH radicals according to the following equation:

$$e^- + O_2 \rightarrow •O_2^- + 2H^+ + 2e^- \rightarrow •OH + OH^- \quad (1)$$

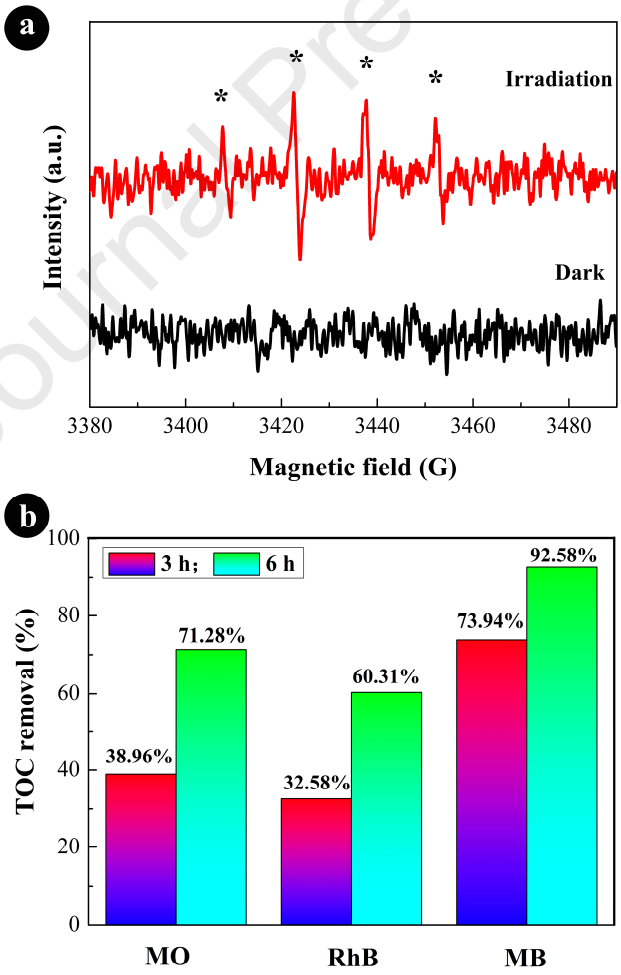

Fig. 9 The ESR (a) and TOC removal (b) of S-10 sample.

The •OH radical formation was testified by the ESR spin-trap technique in Fig. 9a. No ESR signals appear without solar irradiation, and this indicates that the solar irradiation is the precondition of free radical generation. Amazingly, four ESR characteristic peaks with 1:2:2:1 intensity were observed only after 5 min solar irradiation, testifying the formation of DMPO-OH• adduct. However, the characteristic $\bullet O_2^-$ peaks weren't seen under solar irradiation, and the reason is ascribed to the rapid transformation into •OH radicals. Other scientist and our previous results have illuminated the reason in-depth, and the 660 times difference of formation rate limits the long-term stable presence of $\bullet O_2^-$ radicals. Moreover, the mineralization of dyes was carried out by TOC test in Fig. 9b. Except for MB dyes, the mineralization degree of MO and RhB is low, and only less than 40% is completely decomposed. Therefore, the prolonged irradiation time is needed to further improve the dye mineralization, and the mineralization degree is significantly enhanced after 6 h solar irradiation. The 71.28%, 60.31% and 92.58% of MO, RhB and MB mineralization efficiency are obtained after 6 h irradiation , respectively.

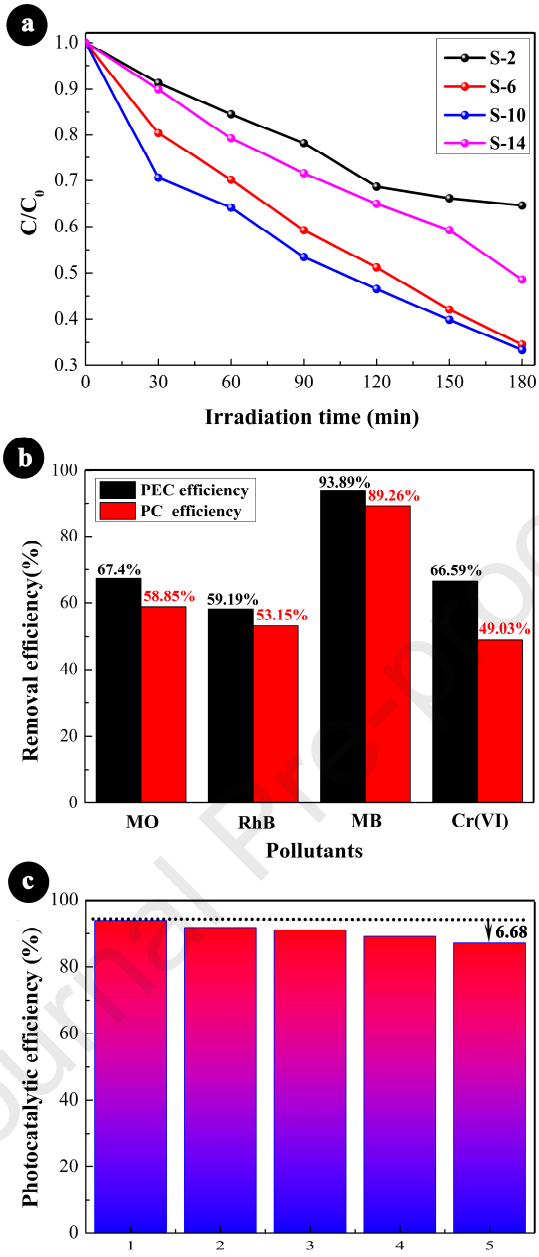

Fig. 10 PEC removal curves of Cr(VI) (a), the contrastive curves of PC and PEC performances (b) and repeated stability (c) of S-10 photocatalyst.

The heavy metal ions Cr(VI) were removed by photocatalytic reduction into Cr(III) with low toxicity, and the photocatalytic performance was displayed in Fig. 10a. The S-10 and S-6 samples exhibited the most excellent photocatalytic capacity, and the final photocatalytic efficiency is 65.48% after 3 h solar irradiation. The S-2 sample shows the weak photocatalytic reduction performance, and only 35.40% of Cr(VI) is

removed. The photocatalytic removal trend of Cr(VI) is similar with that of dye decoloration, and the S-10 photocatalyst exhibits the optimal photocatalytic activity among these samples. The excellent photocatalytic performance of S-10 is largely attributed to the efficient charge carrier separation and transportation, and the external voltage is favorable to the electron transfer. The external voltage influences on the photocatalytic pollutant removal were studied in Fig. 10b, and all pollutant photocatalytic efficiencies show downslide status without external voltage. The external voltage (0.5 V) inhibits the electron recombination, and prolongs the electron life. Furthermore, the photocorrosion stability is also an important index to evaluate the photocatalytic application, and the cyclic photocatalytic performances of S-10 in the MB decoloration were carried out in Fig. 10c. After the fifth photocatalytic experiment, the photocatalytic efficiency is only 6.68% lower than the first one, which indicates the high stability of S-10 samples. The photocatalytic results illuminate that Ag_2O nanoparticles are admirable semiconductor sensitizers for the enhanced photocatalytic performance of TiO_2 NTs, and the suitable deposition amounts by SILAR adjustment in S-10 achieves the brilliance photocatalytic manifestation and prospect in waste water purification. The detailed photocatalytic mechanism was described in Scheme 1b. Firstly, the p-n heterojunction could form at the S-10 photocatalyst surface due to the p-type semiconductor of Ag_2O and n-type characterization of TiO_2 NTA [32, 38]. The collaborative inhibiting roles of built-in electric field and external voltage dramatically accelerate the separation of electrons, and then massive •OH radicals are produced to degrade the dye molecules due to the

superhigh oxidative activity ($\varphi^{\theta}(H_2O/\cdot OH)$= 2.38 V, $\varphi^{\theta}(OH^-/\cdot OH)$= 1.99 V). Finally, organic dyes are decomposed into inorganic species such as CO_2 and H_2O. The photocatalytic reaction progress is described in the following equations. Therefore, the outstanding photocatalytic ability of Ag_2O/TiO_2 NTA would further enhance the application prospect of photocatalysts in industrial waste water treatment.

$$Ag_2O/TiO_2\ NTA + h\nu \rightarrow e_{CB}^- + h_{VB}^+ \quad (2)$$

$$O_2 + e_{CB}^- \rightarrow \bullet O_2^- \quad (3)$$

$$\bullet O_2^- + H_2O \rightarrow \bullet OOH + OH^- \quad (4)$$

$$\bullet OOH + H_2O + e_{CB}^- \rightarrow H_2O_2 + OH^- \quad (5)$$

$$H_2O_2 + e_{CB}^- \rightarrow \bullet OH + OH^- \quad (6)$$

$$h_{VB}^+ + H_2O \rightarrow \bullet OH + H^+ \quad (7)$$

$$h_{VB}^+ + OH^- \rightarrow \bullet OH \quad (8)$$

$$\bullet OH + dyes \rightarrow CO_2 + H_2O \quad (9)$$

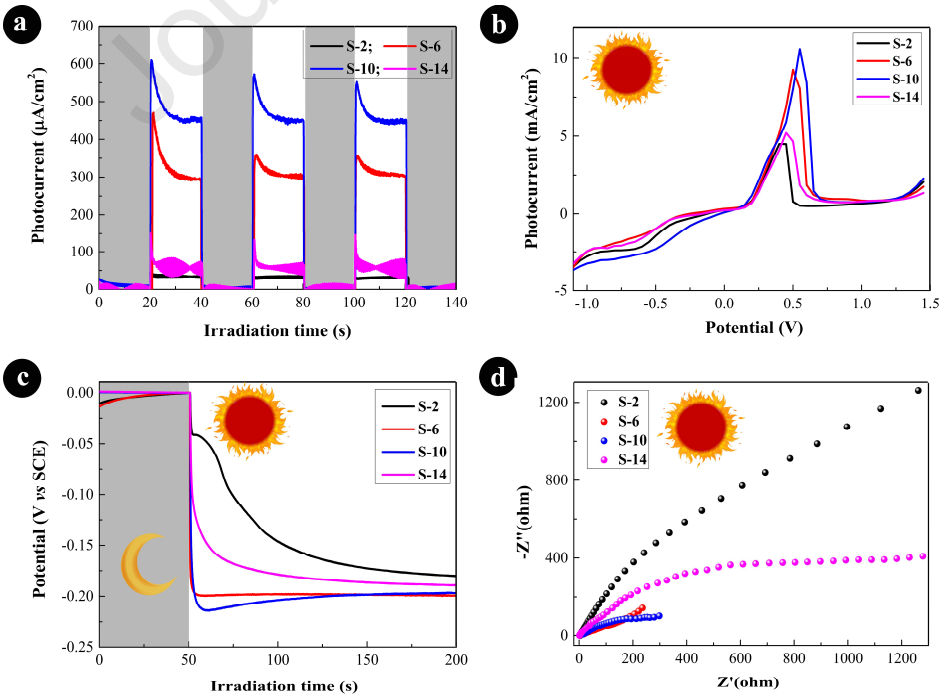

Fig. 11 The transient photocurrent response (a), *I-V* curves (b), OCP (c) and EIS (d)

of the as-prepared photoelectrodes under visible light irradiation.

The visible light-driven photoelectrochemical property of the samples sensitized by Ag_2O nanoparticles was tested in Fig. 11. The transient photocurrent was clearly noticed along the Xe lamp irradiation. All samples displayed strong photoelectrochemical stability without any photocorrosion. The high photocurrent difference could be observed among these samples, and SILAR cycles exhibited remarkable influences on the final photocurrent density. The photocurrent progressively increased from 2 cycles to 10 cycles, and then rapidly decreased in the sample prepared in 14 h. The highest photocurrent in S-10 is calculated to be 463.2 $\mu A/cm^2$, and the photocurrent of S-6 is around 303.5 $\mu A/cm^2$. The visible light photocurrent generation with different adding voltages was displayed in Fig. 11b, and the photocurrent generation trend of these photoelectrodes is identical with that without adding voltages. The photogenerated voltage at electrode surface was tested in Fig. 11c. The S-6 and S-10 photoelectrodes also quickly produce photovoltages, and the value is about -0.20 V. However, the stable state achievement of photovoltage in S-2 and S-14 needs long period, which reflects the weak electron transfer and high interface resistance. Therefore, the photoelectrode resistance of these samples was researched in Fig. 11d, and the small semicircle diameters could be observed in S-6 and S-10 photoelectrodes, which confirms the guess about electron transfer. The high electron transportation and solar harvesting of S-10 photocatalyst would exhibit attractive prospect in waste water treatment and new resource generation.

4. Conclusions

In summary, Ag_2O nanoparticles were deposited on TiO_2 NTA by the SILAR method, and the deposition cycles dramatically influenced the photoelectrochemical performances including visible light photocurrent and photocatalysis. The S-10 sample exhibited the optimal transient photocurrent (463.2 $\mu A/cm^2$) and surface photovoltage (-0.20 V) under visible light irradiation, and MO, RhB, MB dye molecules were decomposed under solar irradiation. The •OH radicals were confirmed to be the decisive active specie for the dye decoloration, and the photocatalyst showed significantly high stability. The excellent photocatalytic capacity of Ag_2O/TiO_2 NTA suggests that the as-prepared photocatalyst has prospective application in waste water remediation.

Acknowledgments

This work was financially supported by Fund for Tianshan Young Scholars (2018Q031), Educational Foundation of Xinjiang Province (XJEDU2018Y060), Natural Science Foundation of Shandong Province (ZR2019QB023, ZR2019MB019) and National Natural Science Foundation of China (51402145).

References

[1] Emrah Ozturk, Mustafa Karaboyacı, Ulku Yetis, Nevzat O.Yigit, Mehmet Kitis, Evaluation of integrated pollution prevention control in a textile fiber production and dyeing mill, J. Clean. Prod., 2015, 88, 116-124.

[2] Mengdi Liu, Ronald Shadbegian, Bing Zhang, Does environmental regulation affect labor demand in China? Evidence from the textile printing and dyeing industry, J. Environ. Econ. Manag., 2017, 86, 277-294.

[3] Jiade Wang, Tian Zhang, Yu Mei, Bingjun Pan, Treatment of reverse-osmosis concentrate of printing and dyeing wastewater by electro-oxidation process with controlled oxidation-reduction potential (ORP), Chemosphere, 2018, 201, 621-626.

[4] Rui Wang, Xin Jin, Ziyuan Wang, Wantao Gu, Zhechao Wei, Yuanjie Huang, Zhuang Qiu, Pengkang Jin, A multilevel reuse system with source separation process for printing and dyeing wastewater treatment: A case study, Bioresource Technol, 2018, 247, 1233-1241.

[5] Longbo Jiang, Xingzhong Yuan, Guangming Zeng, Zhibin Wu, Jie Liang, Xiaohong Chen, Lijian Leng, Hui Wang, Hou Wang, Metal-free efficient photocatalyst for stable visible-light photocatalytic degradation of refractory pollutant, Appl. Catal. B: Environ., 2018, 221, 715-725.

[6] Sheng Wang, Panyong Kuang, Bei Cheng, Jiaguo Yu, Chuanjia Jiang, ZnO hierarchical microsphere for enhanced photocatalytic activity, J. Alloy. Compd., 2018, 741, 622-632.

[7] Feng Zhou, Chunjie Yan, Qi Sun, Sridhar Komarneni, TiO_2/Sepiolite nanocomposites doped with rare earth ions: Preparation, characterization and visible light photocatalytic activity, Micropor. Mesopor. Mat., 2019, 274, 25-32.

[8] Danlian Huang, Zhihao Li, Guangming Zeng, Chengyun Zhou, Wenjing Xue, Xiaomin Gong, Xuelei Yan, Sha Chen, Wenjun Wang, Min Cheng, Megamerger in photocatalytic field: 2D g-C_3N_4 nanosheets serve as support of 0D nanomaterials for improving photocatalytic performance, Appl. Catal. B: Environ., 2019, 240, 153-173.

[9] Qingyao Wang, Huili Li, Xueling Yu, Yao Jia, Yuan Chang, Shanmin Gao, Morphology regulated Bi_2WO_6 nanoparticles on TiO_2 nanotubes by solvothermal Sb^{3+} doping as effective photocatalysts for wastewater treatment, Electrochim. Acta, 2020, 330, 135167.

[10] Zipeng Xing, Jiaqi Zhang, Jiayi Cui, Junwei Yin, Tianyu Zhao, Junyan Kuang, Ziyuan Xiu,

Ning Wan, Wei Zhou, Recent advances in floating TiO_2-based photocatalysts for environmental application, Appl. Catal. B: Environ., 2018, 225, 452-467.

[11] Yin Ye, Harry Bruning, Wanrong Liu, Huub Rijnaarts, Doekle Yntema, Effect of dissolved natural organic matter on the photocatalytic micropollutant removal performance of TiO_2 nanotube array, J. Photoch. Photobio. A, 2019, 371, 216-222.

[12] Zhiyuan Liu, Yadong Song, Qingyao Wang, Yao Jia, Xinying Tan, Xinxin Du, Shanmin Gao, Solvothermal fabrication and construction of highly photoelectrocatalytic TiO_2 NTs/Bi_2MoO_6 heterojunction based on titanium mesh, J. Colloid Interf. Sci., 2019, 556, 92-101.

[13] Longyu Qiu, Qingyao Wang, Zhiyuan Liu, Qianqian Zhao, Xiaoyu Tian, Huili Li, Shanmin Gao, Preparation of 3D TiO_2 nanotube arrays photoelectrode on Ti mesh for photoelectric conversion and photoelectrocatalytic removal of pollutant, Sep. Purif. Technol., 2018, 207, 206-212.

[14] Qingyao Wang, Longyu Qiu, Yao Jia, Yuan Chang, Xinying Tan, Lixia Yang, Hou Chen, Design of carbon loaded porous TiO_2 foams by the hydrothermal-assisted annealing carbonization of fruit residue for solar-driven water evaporation, Sol. Energ. Mater. Sol. C., 2019, 202, 110116.

[15] Zhiyuan Liu, Qingyao Wang, Xinying Tan, Yujie Wang, Rencheng Jin, Shanmin Gao, Enhanced photocatalytic performance of TiO_2 NTs decorated with chrysanthemum-like BiOI nanoflowers, Sep. Purif. Technol., 2019, 215, 565-572.

[16] Zhizhong Liu, Ping Xu, Hao Song, Jiangwen Xu, Jijiang Fu, Biao Gao, Xuming Zhang, Paul K. Chu, In situ formation of porous TiO_2 nanotube array with $MgTiO_3$ nanoparticles for enhanced photocatalytic activity, Surf. Coat. Tech., 2019, 365, 222-226.

[17] Qingyao Wang, Qianqin Yuan, Zhiyuan Liu, Rencheng Jin, Yuming Cui, Shanmin Gao,

Ultrasound-assisted synthesis and solar-light-driven photoelectrocatalytic activity of CdS sensitized TiO_2 nanotube array photocatalysts, Sep. Purif. Technol., 2018, 194, 216-221.

[18] Zhiyuan Liu, Qingyao Wang, Wenqian Rong, Rencheng Jin, Yuming Cui, Shanmin Gao, CTAB assisted hydrothermal preparation of Bi_2WO_6-WO_3 nanosheets on TiO_2 nanotube arrays for photoelectrocatalytic applications, Sep. Purif. Technol., 2018, 200, 191-197.

[19] Xiaoyu Tian, Qingyao Wang, Qianqian Zhao, Longyu Qiu, Xiaofeng Zhang, Shanmin Gao, SILAR deposition of CuO nanosheets on the TiO_2 nanotube arrays for the high performance solar cells and photocatalysts, Sep. Purif. Technol., 2019, 209, 368-374.

[20] Qingyao Wang, Qiaodan Zheng, Rencheng Jin, Shanmin Gao, Qianqin Yuan, Wenqian Rong, Renliang Wang, Photoelectrocatalytic removal of organic dyes and Cr(VI) ions using Ag_3PO_4 nanoparticles sensitized TiO_2 nanotube arrays, Mater. Chem. Phys., 2017, 199, 209-215.

[21] Yuqi Cui, Zixuan Zhang, Bo Li, Ruonan Guo, Xinyi Zhang, Xiuwen Cheng, Mingzheng Xie, Qingfeng Cheng, Ultrasound assisted fabrication of AgBr/TiO_2 nano-tube arrays photoelectrode and its enhanced visible photocatalytic performance and mechanism for detoxification of 4-chlorphenol, Sep. Purif. Technol., 2018, 197, 189-196.

[22] Ming Wu, Hongying Lv, Teng Wang, Zhimin Ao, Hongqi Sun, Chengyin Wang, Taicheng An, Shaobin Wang, Ag_2MoO_4 nanoparticles encapsulated in g-C_3N_4 for sunlight photodegradation of pollutants, Catal. Today, 2018, 315, 205-212.

[23] Haitao Ren, Qing Yang, Fabrication of Ag_2O/TiO_2 with enhanced photocatalytic performances for dye pollutants degradation by a pH-induced method, Appl. Surf. Sci., 2017, 396, 530-538.

[24] Weijia Zhou, Hong Liu, Jiyang Wang, Duo Liu, Guojun Du, Jingjie Cui, Ag_2O/TiO_2 nanobelts

heterostructure with enhanced ultraviolet and visible photocatalytic activity, ACS Appl. Mater. Interfaces, 2010, 2, 2385-2392.

[25] Chengbin Liu, Chenghao Cao, Xubiao Luo, Shenglian Luo, Ag-bridged Ag_2O nanowire network/TiO_2 nanotube array p-n heterojunction as a highly efficient and stable visible light photocatalyst, J. Hazard. Mater., 2015, 285, 319-324.

[26] Xiaoyong Deng, Qiuling Ma, Yuqi Cui, Huixuan Zhang, Xiuwen Cheng, Xiaoli Li, Mingzheng Xie, Qingfeng Cheng, Bo Li, Microwave-assisted synthesis of Ag_2O/reduced TiO_2 nano-tube arrays photoelectrode with enhanced visible photocatalytic activity for degradation of organic pollutants, Sep. Purif. Technol., 182 (2017) 230-237.

[27] Qingyao Wang, Xiaotong Wang, Miao Zhang, Guihua Li, Shanmin Gao, Mingyang Li, Yiqing Zhang, Influence of Ag-Au microstructure on the photoelectrocatalytic performance of TiO_2 nanotube array photocatalysts, J. Colloid Interf. Sci., 2016, 463, 308-316.

[28] Qingyao Wang, Chao Chen, Wei Liu, Shanmin Gao, Xiuchun Yang, Recent progress in all-solid-state quantum dot-sensitized TiO_2 nanotube array solar cells, J. Nanopart. Res., 2016, 18, 7.

[29] Qingyao Wang, Zhiyuan Liu, Rencheng Jin, Ying Wang, Shanmin Gao, SILAR preparation of Bi_2S_3 nanoparticles sensitized TiO_2 nanotube arrays for efficient solar cells and photocatalysts, Sep. Purif. Technol., 2019, 210, 798-803.

[30] Yiou Wang, Anastasia Vogel, Michael Sachs, Reiner Sebastian Sprick, Liam Wilbraham, Savio J. A. Moniz, Robert Godin, Martijn A. Zwijnenburg, James R. Durrant, Andrew I. Cooper, Junwang Tang, Current understanding and challenges of solar-driven hydrogen generation using polymeric photocatalysts, Nat. Energy, 2019, 4, 746-760.

[31] Paweł Mazierski, Anna Malankowska, Marek Kobylanski, Magdalena Diak, Magda Kozak, Michał J. Winiarski, Tomasz Klimczuk, Wojciech Lisowski, Grzegorz Nowaczyk, Adriana Zaleska-Medynska, Photocatalytically active TiO_2/Ag_2O nanotube arrays interlaced with silver nanoparticles obtained from the one-step anodic oxidation of Ti-Ag alloys, ACS Catal., 2017, 7, 2753-2764.

[32] Debabrata Sarkar, Chandan. K. Ghosh, S. Mukherjee, Kalyan K. Chattopadhyay, Three dimensional Ag_2O/TiO_2 type-II (p−n) nanoheterojunctions for superior photocatalytic activity, ACS Appl. Mater. Interfaces, 2013, 5, 331-337.

[33] Weijia Zhou, Hong Liu, Jiyang Wang, Duo Liu, Guojun Du, Jingjie Cui, Ag_2O/TiO_2 nanobelts heterostructure with enhanced ultraviolet and visible photocatalytic activity, ACS Appl. Mater. Interfaces, 2010, 2, 2385-2392.

[34] Xiaoyong Deng, Qiuling Ma, Yuqi Cui, Huixuan Zhang, Xiuwen Cheng, Xiaoli Li, Mingzheng Xie, Qingfeng Cheng, Bo Li, Microwave-assisted synthesis of Ag_2O/reduced TiO_2 nano-tube arrays photoelectrode with enhanced visible photocatalytic activity for degradation of organic pollutants, Sep. Purif. Technol., 2017, 182, 230-237.

[35] Bingkun Liu, Lilong Mu, Bing Han, Jingtao Zhang, Hengzhen Shi, Fabrication of TiO_2/Ag_2O heterostructure with enhanced photocatalytic and antibacterial activities under visible light irradiation, Appl. Surf. Sci., 2017, 396, 1596-1603.

[36] Kamal Kumar Paul, Ramesh Ghosh, P K Giri, Mechanism of strong visible light photocatalysis by Ag_2O-nanoparticle-decorated monoclinic TiO_2(B) porous nanorods, Nanotechnology, 2016, 27, 31.

[37] Osman AhmedZelekew, Dong-Hau Kuo, Jemal Mohammed Yassin, Kedir Ebrahim Ahmed, Hairus Abdullah,Synthesis of efficient silica supported TiO_2/Ag_2O heterostructured catalyst with enhanced photocatalytic performance, Appl. Surf. Sci., 2017, 410, 454-463.

[38] Chenchun Hao, Wenzhong Wang, Ru Zhang, Bin Zou, Honglong Shi, Enhanced photoelectrochemical water splitting with $TiO_2@Ag_2O$ nanowire arrays via p-n heterojunction formation, Sol. Energ. Mater. Sol. C., 2018, 174, 132-139.

Figure captions:

Scheme 1 The preparation (a) and photocatalytic mechanism (b) of Ag_2O/TiO_2 NTA.

Fig. 1 XRD patterns of the samples.

Fig. 2 SEM images of TiO_2 NTA (a) and S-10 (b).

Fig. 3 SEM images of S-2 (a), S-6 (b) S-10 (c) and S-14 (d).

Fig. 4 TEM (a, b), HRTEM images (c) and elemental mappings (d) of S-10.

Fig. 5 XPS spectra of survey (a), Ti 2p (b), Ag 3d (c) and O 1s (d).

Fig. 6 DRS spectra (a), IPCE (b) and PL (c) of the as-prepared samples.

Fig. 7 PEC degradation of MO (a), RhB (b) and MB (c) by the as-prepared photocatalysts.

Fig. 8 The photocatalytic performance after adding scavengers in MO (a), RhB (b) and MB (c) solutions.

Fig. 9 The ESR (a) and TOC removal (b) of S-10 sample.

Fig. 10 PEC removal curves of Cr(VI) (a), the contrastive curves of PC and PEC

performances (b) and repeated stability (c) of S-10 photocatalyst.

Fig. 11 The transient photocurrent response (a), *I*-*V* curves (b), OCP (c) and EIS (d) of the as-prepared photoelectrodes under visible light irradiation.

Highlights

1. Ag_2O nanoparticles were deposited on TiO_2 NTA by a SILAR method.

2. The Ag_2O/TiO_2 NTA showed the attractive photocatalytic activity.

3. The active group and photocatalytic mechanism were investigated.

Conflict of interest statement

The authors declared that there is no conflict of interest.